Contrib. Plasma Phys. **44**, No. 7-8, 589 – 593 (2004) / **DOI** 10.1002/ctpp.200410086

PIC-MCC Modeling of a Capacitive RF discharge

K. Matyash[*] and **R. Schneider**

Max-Planck-Institut für Plasmaphysik,Teilinstitut Greifswald, Wendelsteinstr.1, D-17491 Greifswald, Germany

Received 15 April 2004, accepted 15 April 2004
Published online 29 October 2004

Key words Particle-in-Cell method, plasma heating by radio-frequency fields.
PACS 52.65.Rr, 52.50.Qt

1 Introduction

Capacitive radio frequency (RF) discharges are very popular, both in laboratory research for the production of low-temperature plasmas, and industry, where they are commonly used for thin film deposition and surface etching [1–3].

Although the experimental set-up for capacitive RF discharge seems to be rather simple, the discharge itself is inherently complex. In such discharges the physics of a non-equilibrium non-stationary plasma is combined with the complexity of reactive plasma processes, including the surface interaction, which makes the modeling of such systems a real challenge. Despite the numerous experimental and theoretical studies performed on RF capacitive discharges (see, for example, [2] and references contained therein), the understanding of its behavior is still far from complete. Particle models were recently successfully applied for modeling of capacitive RF discharges in helium [4], hydrogen [5] and argon [6, 7] and proved to be a promising tool for simulation of such plasmas, providing insight into discharge parameters which are difficult to measure experimentally.

2 PIC-MCC model

We used the electrostatic 2D3V Particle-in-Cell (PIC) code with Monte-Carlo collisions [8] to model a capacitive RF discharge in a methane-hydrogen mix, similar to one described in [9]. In this model electrons and ions are treated as particles, moving in self-consistent electric field. 2 spatial and 3 velocity components are used, and a binary Monte-Carlo Coulomb collision model for electron-electron, electron-ion and ion-ion collisions is applied. Inter-species reactions are included by application of the binary inelastic collision model.

In the simulations the initial electron density and temperature were chosen as $n_{e0} = 10^{10}\,cm^{-3}$ and $T_{e0} = 10\,eV$ respectively (Maxwellian distribution and uniform density was assumed). The mix of CH_4 and H_2 was used as a background gas. The gas temperature, $T_n = 500\,K$, and densities, $n_{CH_4} = 7 \cdot 10^{14}\,cm^{-3}$, $n_{H_2} = 9.2 \cdot 10^{14}\,cm^{-3}$, were chosen close to those used in [9], the total pressure of the background gas was $p = 11.24\,Pa$ (0.085 Torr). A rectangular domain with the length $d = Y_{max} = 128 \cdot \lambda_{D0} = 4.25\,cm$ and the width $X_{max} = 8 \cdot \lambda_{D0} = 0.19\,cm$ was used. In the Y direction at positions of the electrodes $Y = 0$ and $Y = Y_{max}$ the absorbing wall boundary conditions were applied. The potential at $Y = Y_{max}$ was fixed at zero, corresponding to the grounded electrode. At the position of the powered electrode at $Y = 0$ the potential was assumed to oscillate harmonically according to applied RF voltage: $\phi(0, t) = U_{RF} \sin(\omega_{RF})$ with $\omega_{RF}/2\pi = 13.56\,MHz$. At the boundaries in the X direction a periodic boundary condition was applied. As neutral species densities are much larger than densities of charged species, the neutral species were treated as background with fixed density and temperature. Only the dynamics of charged particles was followed. In order to obtain an accurate electron

[*] Corresponding author: e-mail: Konstantin.Matyash@ipp.mpg.de, Phone: +49 3834 882400, Fax: +49 3834 882409

energy distribution, the comprehensive list of electron-neutral reactions for CH_4 and H_2 was added in the model, including the rotational, vibrational and electronic excitation as well as dissociation and ionization collisions and the elastic scattering. Cross-sections for these collisional processes were collected from the compilation used in [9].

In calculations a grid size $\Delta x = \lambda_{D0}/2 = 0.017\,cm$ and time step $\Delta t = 0.2/\omega_{pe} = 3.55 \cdot 10^{-11} s$ was used. The number of computational particles per Debye cell was chosen as $N_d = 1000$, totaling about $4 \cdot 10^6$ computational particles used in the simulation. The simulation covered a few thousand RF cycles in order to ensure that the discharge reached equilibrium. The equilibration time was determined by the longest time scale in the system - the ion transit time, which was a few hundred RF cycles. The calculations were carried out on a 16-processor Linux cluster in about 50 hours.

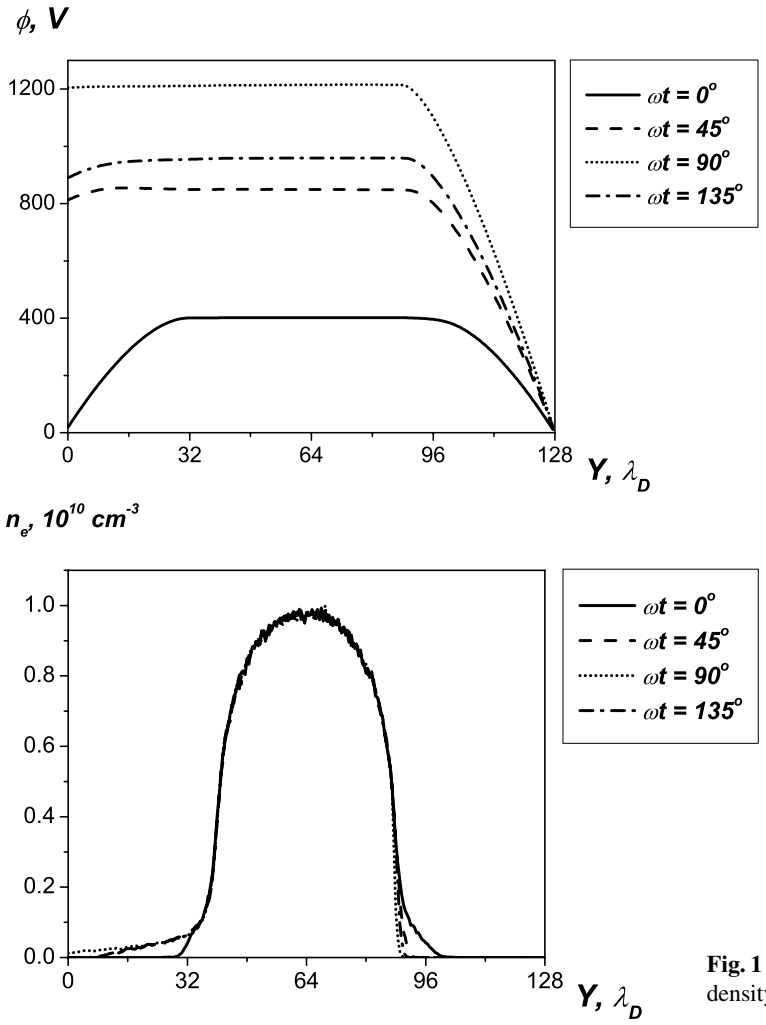

Fig. 1 Dynamics of potential (top) and the electron density (bottom) over RF cycle ($p = 0.085\,Torr$).

3 Results and discussion

In Fig 1 the dynamics of potential and the electron density in the system during the RF cycle is presented. We can see that a steep potential drop, up to $\Delta\phi_{max} \approx 1100\,V$, takes place near the electrodes within oscillating positive space-charge layers of about $L_s \approx 32 \cdot \lambda_{D0}$ thick - the RF sheaths. The strong electric field in the RF sheath regions is directed toward the electrodes, preventing electrons from leaving the plasma for most of the RF cycle. The electrons are able to escape to electrodes only during a short time, when the RF sheath collapses. The ions due to high inertia are not able to react to the fast changing RF electric field. On their timescale ions respond

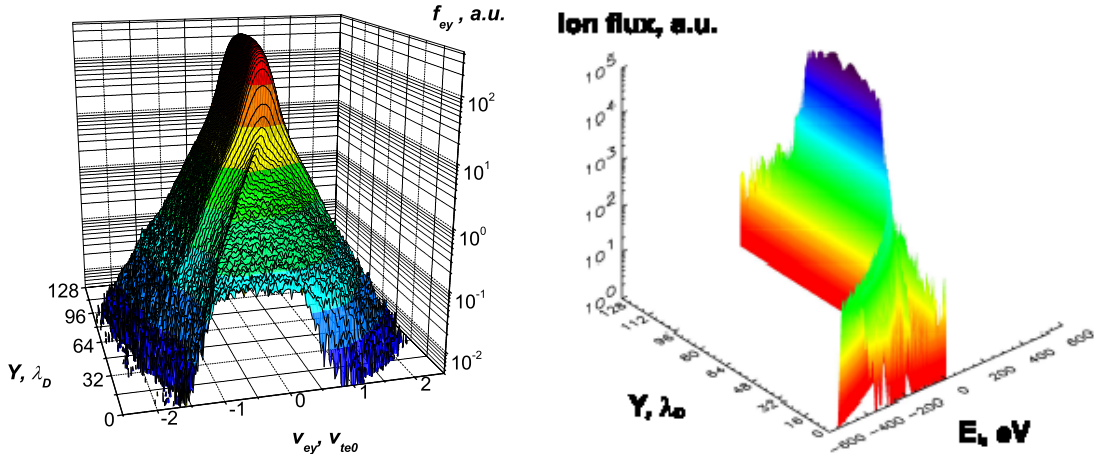

Fig. 2 Profiles of electron parallel velocity component distribution (top) and the spectrum of the parallel CH_4^+ ion energy (bottom) averaged over the RF cycle ($p = 0.085\,Torr$). (Online colour:www.cpp-journal.org).

only to the electric field averaged over RF cycle, such that the flux of energetic ions, accelerated in the sheath electric field to energies of about average sheath potential drop, constantly flows to the electrodes.

In Fig. 2 we plot the electron parallel velocity component distribution and the spectrum of the parallel CH_4^+ ion energy depending on the longitudinal coordinate Y, both averaged over the RF cycle. In the electron distribution we can distinguish two groups: the time independent formation of cold electrons in the middle of system, and the tail of high-energy electrons oscillating between the electrodes. The electrons from the low energy group (with average energy about $0.2\,eV$) are not energetic enough to overcome the presheath ambipolar potential, thus they are locked in the middle of the system. The electrons from the high-energy tail can easily penetrate into the sheath regions. As in our case the mean free path for electron-neutral elastic collisions $\lambda_{en} \approx \frac{1}{n_n \sigma_e n} \approx 0.5\,cm$ is the same order of magnitude as the system length, these electrons can oscillate between the RF sheaths, getting reflected from them by the strong retarding electric field. Although during single reflection from the sheath, an electron can both gain and loose energy, depending on the phase of the RF field, but on average, electrons are accelerated due to stochastization of their motion, following the Fermi acceleration mechanism [10, 11].

In the ion energy distribution we can see how ions are accelerated in the sheaths toward the wall. A saddle-like structure in the ion energy distribution at the wall position with two peaks at energies $430\,eV$ and $530\,eV$ is caused by RF modulation of the ions which experience the full sheath potential drop. The peaks at lower energies are contributed by low-energy ions produced due to collisions inside the sheath. The number of the secondary branches corresponds to the number of RF periods that an ion takes to cross the sheath.

In order to study the influence of the electron-neutral collisions on discharge behavior, we performed a simulation for background gas pressure, increased by a factor of 10 (0.85 Torr), with neutral densities $n_{CH_4} = 7 \cdot 10^{15}\,cm^{-3}$ and $n_{H_2} = 9.2 \cdot 10^{15}\,cm^{-3}$.

In Fig 3. the dynamics of potential during the RF cycle and averaged electron parallel velocity distribution is presented. We can see that, in the case of higher pressure, the collapse of the RF sheath leads to the reversal of electric field in the sheath region. During the short interval of the RF cycle, the electric field in the sheath region changes direction and accelerates electrons toward the electrode. Because electrons reach the electrode only during the short time when the sheath collapses, in the case of high working gas pressure, when electron mobility is reduced due to electron-neutral collisions, the accelerating electric field is necessary at this time to provide electron current sufficient to keep balance with generally constant ion current. In the electron velocity distribution we can see that heating of electrons takes place in the sheath regions near the electrodes. The mean free path of electron-neutral elastic collisions is now $\lambda_{en} \approx 0.05\,cm$, which is much smaller than the system length and considerably smaller then the sheath width $L_s \approx 0.5\,cm$. Thus, the Ohmic heating in the sheath region, when the electrons are accelerated in the strong electric field between successive elastic collisions with neutrals, becomes the dominating mechanism of electron heating. Electrons are heated in both half-periods of

the RF cycle: during sheath expansion and reversal of the sheath electric field. The mean free path for electron-neutral inelastic collisions $\lambda_i \approx 0.5\,cm$ is close to the sheath width, so electrons are quickly cooled down by inelastic collisions after they leave the sheath region.

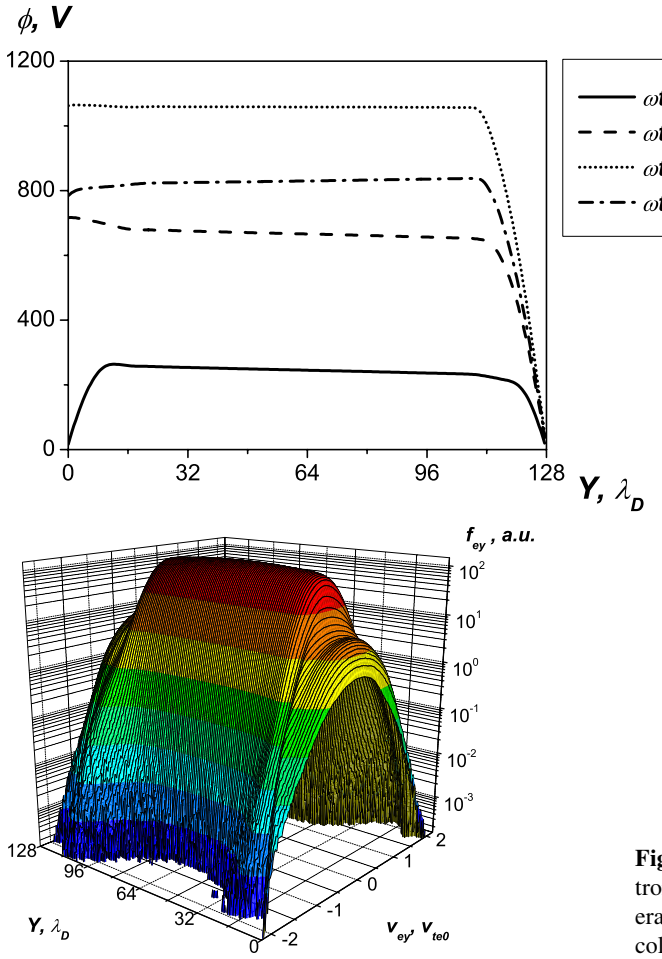

Fig. 3 Dynamics of potential (top) and profile of electron parallel velocity component distribution (bottom) averaged over the RF cycle ($p = 0.085\,Torr$). (Online colour:www.cpp-journal.org).

In Fig. 4 we present the time-resolved electron-impact ionization rate close to the electrode during one RF cycle. Here we can see that the ionization peak near the electrode takes place at time when the electric field near the wall is reversed, and the ionization peak at the sheath edge appears when the repulsive RF sheath builds up. Similar effect of double emissive layers near the electrodes was observed in experiments with capacitive RF discharges [12].

In order to investigate the transition of the electron heating mechanism with the increase of background gas pressure, we performed simulations for the same H_2-CH_4 1.3:1 mix, changing the gas pressure. In Fig. 5 we summarize these simulations, presenting electron energy probability functions (EEPF's) averaged over the RF cycle in the bulk plasma for gas pressures from $0.028\,Torr$ to $0.85\,Torr$. At low pressures the EEPFs are essentially bi-Maxwellian, revealing the stochastic electron heating mechanism, leading to the formation of cold bulk and oscillating hot tail electrons. With increase of the neutral gas pressure between $0.34\,Torr$ and $0.85\,Torr$ EEPF transforms to a convex, Druyvesteyn-type distribution with a high-energy part depleted by inelastic collisions, corresponding to a regime when the Ohmic heating in the sheath regions is the dominant mechanism of the electron heating. Similar changes of electron energy distribution depending on pressure of neutral gas were observed experimentally in capacitive RF discharges [7, 13, 14].

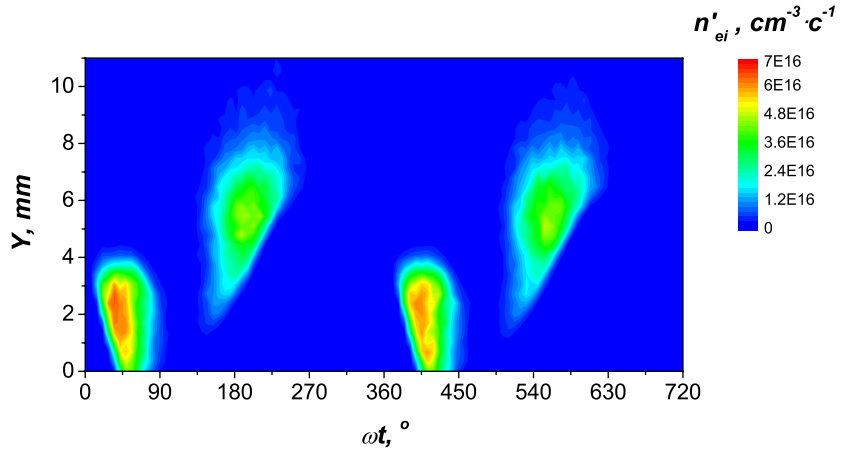

Fig. 4 Spatiotemporal distribution of ionization rate in the vicinity of the electrode ($p = 0.085\,Torr$). (Online colour:www.cpp-journal.org).

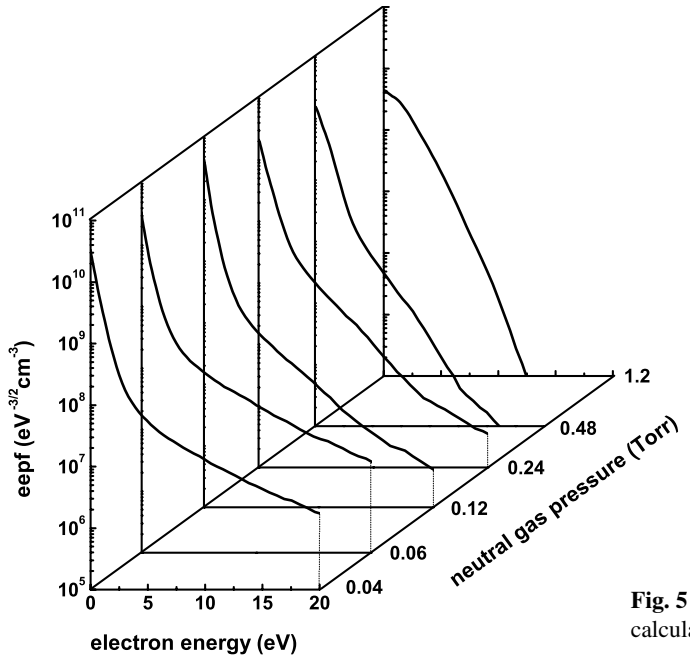

Fig. 5 The electron energy probability functions (EEPF's) calculated for various pressures of CH_4 - H_2 mix.

References

[1] M.A. Lieberman, A.J. Lichtenberg: Principles of Plasma Discharges and Materials Processing, Wiley, New York, 1994.
[2] Y.P. Raizer, M.N. Shneider, N.A. Yatsenko: Radio-Frequency Capacitive Discharges, CRC Press, Boca Raton, London, Tokyo, 1995.
[3] A. Bogaerts, E. Neyts , R. Gijbels, J. van der Mullen, Spectrochimica Acta B **57**, 609 (2002).
[4] M. Surendra, D.B. Graves, I.J. Morey, Appl. Physics. Lett. **56**, 1022 (1990).
[5] D. Vender, R.W. Boswell, J. Vac. Sci. Technol. A **10**, 1331 (1992).
[6] V. Vahedi, G. DiPeso, C.K. Birddall, M.A. Lieberman, T.D. Roglien, Plasma Sources Sci. Technol. **2**, 261 (1993).
[7] M.M. Turner, R.A. Doyle, M.B. Hopkins, Appl. Phys. Lett. **62**, 3247 (1993).
[8] K. Matyash, R. Schneider, A. Bergmann, W. Jacob, U. Fantz, P. Pecher, J. Nucl. Matter. **313-316**, 434 (2003).
[9] C. Busch, Ph.D. thesis, Ruhr-Universitt Bochum, Germany 1999.
[10] V.A. Godiak, Zhurnal Technicheskoy Fiziki **41**, 1364 (1971); see also, Sov. Phys.-Tech. Phys. **16**, 1073 (1972).
[11] M.A. Lieberman, V.A. Godyak, IEE Trans. Plasma. Scie. **26**, 955 (1998).
[12] C.M.O. Mahony, R. Al Wazzan, W.G. Graham, Appl. Phys. Lett. **71**,608 (1997).
[13] V.A. Godyak, R.B. Piejak, Phys. Rev. Lett. **65**, 996 (1990).
[14] V.A. Godyak, R.B. Piejak, B.M. Alexandrovich, Plasma Sources Sci. Technol. **1**, 36 (1992).